Long Atmospheric Waves and the Polar-Plane Approximation to the Earth's Spherical Geometry

ALISON F. C. BRIDGER AND DUANE E. STEVENS

Department of Atmospheric Science, Colorado State University, Fort Collins 80523

(Manuscript received 8 August 1979, in final form 22 October 1979)

ABSTRACT

The spherical geometry of the earth is replaced by polar cylindrical geometry, with a plane tangential to the earth at the pole. The resulting frequency and structure of free motions in an isothermal, adiabatic atmosphere with a resting basic state is studied in both geometries. The solutions for v (meridional wind) may be written as a single Bessel function if certain approximations are made. For positive equivalent depths, the geometrical approximation is best when the Lamb parameter $\epsilon \geq 10$, so that Rossby waves are well modeled, while fast moving gravity waves are not well approximated. The impact of setting f to a constant value when undifferentiated, as in the usual midlatitude beta-plane approximation, is examined. It is found that the value of f is as important in determining how well the model behaves as are the geometrical and other approximations.

1. Introduction

In studies of the largest scale of atmospheric waves, the spherical shape of the earth should be taken into account. However, even the most trivial problem, which concerns free motions in an isothermal atmosphere with a resting basic state, quickly becomes mathematically intractable. The horizontal structure functions (Hough functions) are customarily written as an infinite sum of associated Legendre polynomials and the corresponding equation for the frequency of a given disturbance is then an infinite polynomial. Methods of bypassing this problem are widely reported in the literature. Longuet-Higgins (1968) truncated the infinite series and was able to solve for the frequencies of free modes as a function of the Lamb parameter ϵ (all symbols are defined in the Appendix). He also showed the structure of the resulting Hough functions. An alternative procedure is to replace the earth's spherical geometry with a simpler geometry, in which the equations of motion yield a simplified horizontal structure equation. Lindzen (1967) adopted this approach in studying both midlatitude and equatorial β planes. Global-scale motions can then be considered as a combination of a midlatitude and an equatorial part.

The usual midlatitude β plane is not completely adequate in representing motions confined to higher latitudes, since it cannot accommodate the convergence of meridians toward the pole. In this paper, we consider the ability of a simplified geometry, that of a plane tangential to the earth at the pole (i.e., polar cylindrical geometry), to model large-scale disturbances at higher latitudes. Since now the horizontal coordinates are radius from pole and longitude, the effect of converging meridians is included. Furthermore, it is not necessary to assume that β is constant in the polar-plane geometry.

Some work along these lines has already been presented by Haurwitz (1975a,b) and is extended here to show a comparison not only of the frequencies of modes in the two geometries, but also of the resulting horizontal structure, i.e., wind and geopotential. It is shown that the polar plane is an acceptable approximation to the sphere at higher latitudes. As such, the polar plane geometry may be a useful tool in the study of such disturbances.

2. Analysis on the sphere

For an adiabatic, hydrostatic atmosphere with no basic state motion, the governing linearized equations for the perturbations on the sphere are

$$\frac{\partial u'}{\partial t} - fv' = \frac{-1}{a\cos\theta}\frac{\partial \Phi'}{\partial \lambda}, \tag{2.1}$$

$$\frac{\partial v'}{\partial t} + fu' = \frac{-1}{a}\frac{\partial \Phi'}{\partial \theta}, \tag{2.2}$$

$$\frac{1}{a\cos\theta}\frac{\partial u'}{\partial \lambda} + \frac{1}{a\cos\theta}\frac{\partial (v'\cos\theta)}{\partial \theta} + \frac{\partial w'}{\partial z} - w' = 0, \tag{2.3}$$

$$\frac{\partial^2 \Phi'}{\partial t \partial z} + w'\Gamma = 0, \tag{2.4}$$

0022-4928/80/030534-11$06.75

where Γ, which is related to the buoyancy frequency, is defined as

$$\Gamma = \left(\frac{d\bar{T}}{dz} + \kappa\bar{T}\right)R^*.$$

Eliminating w' between (2.3) and (2.4) and assuming

$$\begin{pmatrix} u' \\ v' \\ \Phi' \end{pmatrix} \propto e^{i(\sigma t + s\lambda)} \begin{pmatrix} U(\theta)Y(Z) \\ V(\theta)Y(Z) \\ \Psi(\theta)Y(Z) \end{pmatrix}$$

yields the vertical structure equation

$$\left(\frac{d}{dz} - 1\right)\left(\frac{1}{\Gamma}\frac{dY}{dz}\right) + \frac{Y}{gh} = 0,$$

where the separation constant h is the equivalent depth, and also gives the three horizontal structure equations, which may be reduced to Laplace's tidal equation,

$$\frac{d}{d\mu}\left[\frac{(1-\mu^2)}{(\bar{\sigma}^2-\mu^2)}\frac{d\Psi}{d\mu}\right] - \frac{1}{(\bar{\sigma}^2-\mu^2)} \times \left[\frac{s}{\bar{\sigma}}\frac{(\bar{\sigma}^2+\mu^2)}{(\bar{\sigma}^2-\mu^2)} + \frac{s^2}{1-\mu^2}\right]\Psi + \epsilon\Psi = 0, \quad (2.5)$$

where the nondimensional frequency, $\bar{\sigma} = \sigma/2\Omega$, $\mu = \sin\theta$ and $\epsilon = 4\Omega^2a^2/(gh)$ is the Lamb parameter.

A solution to (2.5) is the Hough function

$$\Psi_n^s = \sum_{m=s}^{\infty} C_{n,m}^s P_m^s, \quad (2.6)$$

where $\{P_m^s\}$ are the associated Legendre polynomials, $\{C_{n,m}^s\}$ are expansion coefficients and n is the meridional mode index. Substitution of (2.6) in (2.5) leads to an infinite-order polynomial in the eigenvalue $\bar{\sigma}$. With a few exceptions (see Chapman and Lindzen, 1970), we can proceed no further in the analytical study without considering infinite series. To date, two approaches involving approximations have been adopted to continue the study. First, numerical solutions have been obtained, essentially by truncating the infinite series (2.6). The most extensive such study is that of Longuet-Higgins (1968), who documented both the relationships between $\bar{\sigma}$ and ϵ and the resulting eigenfunctions for varying equivalent depths, both positive and negative. Flattery (1967) gives a similar tabulation of eigenvalues (ϵ) for certain frequencies associated with tidal forcing. He also tabulates expansion coefficients of Hough functions (in terms of associated Legendre polynomials) and the latitudinal structure of these functions for the tidal motions. The second approach has been to approximate the spherical geometry of the earth, usually replacing it with a β plane on which the Coriolis parameter is taken to vary linearly with latitude, wherever its derivative appears. Lindzen (1967) studied both equatorially centered and midlatitude β planes. Their introduction leads to an equivalent form of (2.5), the solution of which can be written as a single known function (Hermite polynomial in the infinite equatorial case, sinusoidal functions in the midlatitude case). Furthermore, the equation governing the relationship between $\bar{\sigma}$ and h reduces to a cubic in $\bar{\sigma}$, when h is specified. Hence the analysis is much simplified and results are readily accessible.

Since the use of the β plane requires an approximation involving the latitudinal extent of the wave disturbance, its applicability is obviously limited. As Holton (1975) points out, the equatorial β plane approximation may be acceptable out to $|y| \approx a$; so that motions confined within the region $-a \leqslant y \leqslant a$ may be studied. Similarly, motions confined to a limited meridional extent in the midlatitudes may be studied on the midlatitude β plane. Consequently, motions which are of greater meridional extent than the geometry can reasonably accommodate cannot be studied on a single β plane. There are two further shortcomings of the β plane. First, β is assigned a constant value, whereas in reality it varies as cos (latitude). Second, the geometrical effect of the convergence of meridians at high latitudes is not accommodated, so that deviations from the true (spherical) results become large as the pole is approached. For the representation of spherical modes, Lindzen (1967) considered both the equatorial and midlatitude β planes. This "multiple β plane" approach has been examined more recently by Thomas and Lux (1978). Again, however, they noted the problem of distortion near the pole.

For certain atmospheric problems, for example, sudden stratospheric warmings and stratospheric waves in high latitudes, such distortions cannot be tolerated. Matsuno (1970, 1971) reverted to spherical geometry in his study of such high-latitude events, as did Dickinson (1968b), whereas Thomas and Lux (1978) proposed using a sequence of β planes to overcome distortion at high latitudes (each β plane is tangential to the sphere at θ_i and on it, the east-west coordinate is given by $x = a\lambda\cos\theta_i$; thus toward the poles, the distance between meridians shrinks). In this paper, we investigate a different approximation to the spherical geometry, which not only incorporates the effect of the convergence of meridians, but also allows β to vary with latitude, while retaining the simplicity of the usual β plane analysis. Haurwitz (1975a,b) presented some results derived in this geometry for both nondivergent and divergent motions in a barotropic atmosphere. A similar approximation was introduced by LeBlond (1964). However, he was interested primarily in very long period motions in a polar, oceanic basin confined to within a radius of 1500 km from the pole, whereas

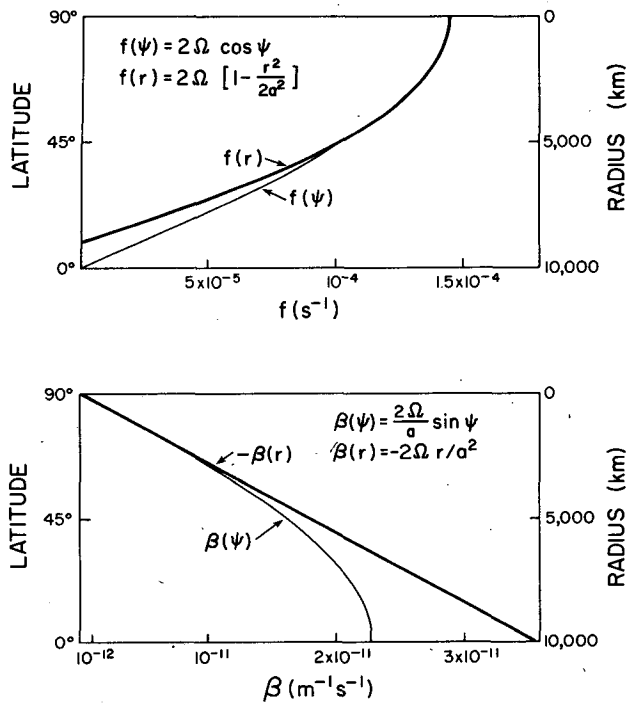

FIG. 1. The variation of f and β with ψ and r in spherical and polar geometries, respectively.

we are interested in higher frequency and larger scale motions typical of the atmosphere. Simmons (1974), in a study of planetary-scale disturbances in a model high-latitude winter stratosphere, which included both vertical and horizontal wind shear, used both the conventional β plane and the polar-plane geometry. The convergence of meridians reduces the local wavelength of disturbances, forming a barrier to propagation (see also Dickinson, 1968a). On the β plane, disturbance maxima were located at the same latitudes as the basic state zonal wind maxima (see his Fig. 3). The introduction of the polar-plane geometry resulted in disturbance maxima shifting to about 5° equatorward of the zonal wind maxima (see his Fig. 4).

3. The polar-plane approximation

The spherical geometry is replaced by polar cylindrical geometry. The coordinates are now r (distance on the sphere from the pole), λ (longitude) and $z = -\ln(p/p_0)$. In terms of ψ (colatitude), r is defined by $r = a\psi$. (Strictly speaking, on the polar plane, $r = a \sin\psi$. The approximation $\sin\psi \approx \psi$ has been made in defining r.) Expanding f in a Taylor series about the pole gives

$$f = 2\Omega \cos\psi = 2\Omega\left[1 - \frac{\psi^2}{2!} + \frac{\psi^4}{4!} - \cdots\right]. \tag{3.1}$$

For small ψ [$\psi \approx 1$ gives $(\psi^4/4!)/(\psi^2/2!) \approx 0.1$], we can write

$$f \approx 2\Omega\left(1 - \frac{r^2}{2a^2}\right), \tag{3.2}$$

so that

$$\beta = \frac{df}{dr} \simeq -\frac{2\Omega r}{a^2}. \tag{3.3}$$

Note that since r increases away from the pole, the sign of $\beta(=df/dr)$ is reversed from that of the conventional $\beta(=df/dy)$. The error in (3.2) is $\leqslant 10\%$ out to $r \approx a$, and β is in error by 20% at $r = a$. Retention of the next term in the approximation to f would reduce both of these errors to under 1%. Fig. 1 shows the variation of f and β in both spherical and polar plane geometries.

The equations corresponding to (2.1)–(2.4) in polar plane geometry are

$$\frac{\partial v_\lambda'}{\partial t} + f v_r' = -\frac{\partial \Phi'}{r\partial\lambda}, \tag{3.4}$$

$$\frac{\partial v_r'}{\partial t} - f v_\lambda' = -\frac{\partial \Phi'}{\partial r}, \tag{3.5}$$

$$\frac{\partial (r v_r')}{r\partial r} + \frac{\partial v_\lambda'}{r\partial\lambda} + \frac{\partial w'}{\partial z} - w' = 0, \tag{3.6}$$

$$\frac{\partial^2 \Phi'}{\partial t \partial z} + w'\Gamma = 0. \tag{3.7}$$

Proceeding as in Section 2, and henceforward deleting primes, we assume

$$\begin{pmatrix} v_r \\ v_\lambda \\ \Phi \end{pmatrix} \propto e^{i(s\lambda+\sigma t)} \begin{pmatrix} R(r)Z(z) \\ \Lambda(r)Z(z) \\ \phi(r)Z(z) \end{pmatrix}.$$

Along with the same vertical structure equation as on the sphere, the horizontal structure equation becomes

$$\frac{d^2R^*}{dr^2} + \frac{(1+\eta^2r^2)}{(1-\eta^2r^2)}\frac{1}{r}\frac{dR^*}{dr} + \left[\frac{2\Omega s}{\sigma a^2} - \frac{2\sigma f}{sgh(1-\eta^2r^2)} - \frac{(f^2-\sigma^2)}{gh} - \frac{s^2}{r^2}\right]R^* = 0, \tag{3.8}$$

where again h is the separation constant, $\eta^2 = \sigma^2/(s^2gh)$ and $R^* = rR$.

It may be noted that Eq. (3.8) may be derived directly from the tidal equations on the sphere [(7.2) in Longuet-Higgins] by making the assumption that colatitude is small.

If (i) f is assumed constant when not differentiated

(as in the midlatitude β plane approximation) and (ii) $\eta^2 r^2 \ll 1$, we can write

$$\frac{d^2R^*}{dr^2} + \frac{1}{r}\frac{dR^*}{dr} + \left[\frac{2\Omega s}{\sigma a^2} - \frac{2\sigma f}{sgh} - \frac{(f^2 - \sigma^2)}{gh} - \frac{s^2}{r^2}\right]R^* = 0, \qquad (3.9)$$

which is Bessel's equation.

The consequences of assumption (i) are discussed in Section 4. For some insight into the second assumption, note that

$$\eta^2 r^2 = \left[\frac{\sigma}{sa^{-1}(gh)^{1/2}}\right]^2 \left(\frac{r}{a}\right)^2.$$

Here $\sigma/sa^{-1}(gh)^{1/2}$ is the ratio of the wave frequency to the frequency of a pure gravity wave with wavenumber s in an ocean of depth h at the equator (as latitude increases, the ratio decreases, all else being fixed). Hence we can only expect the approximation $\eta^2 r^2 \ll 1$ to hold for the low-frequency modes. For example, a rotational free mode on the sphere, with $h = 10$ km, zonal wavenumber $s = 2$ and longitudinal wavenumber $l = 3$ (l is the number of nodes in v_r between poles on the sphere), has a frequency $\sigma \approx 2\pi/(8.5$ days) (Longuet-Higgins, 1968); thus even as far away as the equator ($r \approx 10\,000$ km), $\eta^2 r^2 \approx 0.02$. Our analysis is therefore valid, so long as we are not interested in fast gravity waves. This shortcoming might preclude the use of the model in initial value problems, where the initial state is projected onto a complete set of basic state eigenfunctions. For $h > 0$, we shall henceforward confine our attention to the low-frequency solutions.

Note that the condition $\eta^2 r^2 \ll 1$ may also be written as

$$\eta^2 r^2 \equiv \Delta = \frac{\epsilon\bar{\sigma}^2}{s^2}\left(\frac{r}{a}\right)^2 \ll 1.$$

Thus, for a given wavenumber and at a given radius r, we can plot the curve $\epsilon\bar{\sigma}^2 = (sa/r)^2\Delta$, where $\Delta \ll 1$. The approximation $\eta^2 r^2 \ll 1$ will then hold for all points $(\epsilon,\bar{\sigma})$ in the area lying between the curve and the axes. Fig. 2 shows this relationship for the wave $s = 2$, with $\Delta = 0.1$ and $r = a/2$, a, $3a/2$, all for positive ϵ and $\bar{\sigma}$ (similar curves can be drawn in the other three quadrants). These curves clearly indicate that the fast gravity wave solutions (when $h > 0$) will not be well represented in the polar plane geometry.

The solution of (3.9) is thus

$$R^* = AJ_s(mr) + BY_s(mr),$$

where J and Y are Bessel functions of the first and second kind, respectively, and

$$m^2 = \frac{2\Omega s}{\sigma a^2} - \frac{2\sigma f}{sgh} - \frac{(f^2 - \sigma^2)}{gh} = \text{constant} \qquad (3.10)$$

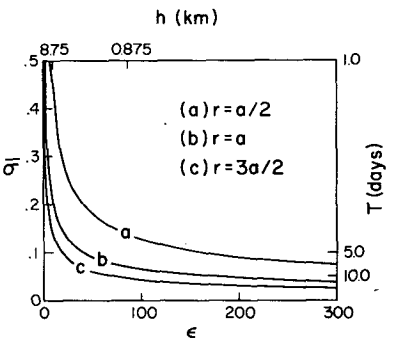

FIG. 2. Plot of $\epsilon\bar{\sigma}^2 = (sa/r)^2\Delta$, where $\Delta = 0.1$, $s = 2$ and $r = a/2$, a and $3a/2$. Points $(\epsilon,\bar{\sigma})$ in the area between the curves and the axes satisfy the approximation $\eta^2 r^2 \leq 0.1$ ($\ll 1$).

when f is taken to be constant. The first term on the right-hand side is $-\beta s/\sigma r$. Requiring boundedness of v_r at the pole, we have $B = 0$ and thus

$$v_r = \frac{AJ_s(mr)}{r} Z(z)e^{i(s\lambda+\sigma t)}, \qquad (3.11)$$

where

$$\lim_{x\to 0} J_s(x) = \frac{(\frac{1}{2}x)^s}{s!} \quad \text{(Abromowitz and Stegun, 1964)}$$

ensures v_r remains finite as $r \to 0$ for all $s \geq 1$. The $s = 0$ case is discussed in Section 4f. We note that this boundary condition produces a behavior of the solutions at the pole similar to that on the sphere, namely, for $s > 1$, $v_r = 0$ at the pole, while for $s = 1$, $dv_r/dr = 0$ at the pole. On the midlatitude β plane (e.g., Lindzen, 1967), it is necessary to impose these different boundary conditions for $s = 1$ and for $s > 1$ to produce the same behavior at the pole as on the sphere. Expressions for v_λ and Φ can be obtained from the set (3.4)–(3.7).

Having reformulated the problem in a different geometry, we must now examine how well the results on the sphere are reproduced.

4. Comparison of solutions

a. Mathematical comparison

Since exact analytical solutions to (2.5) are not available, except in the limiting cases as $|\epsilon| \to \infty$ and as $\epsilon \to 0$, no exact analytical comparisons between the two geometries for arbitrary ϵ are possible. We note, however, that (3.9) $\times r$ is in Sturm-Liouville form. Hence we know that 1) the eigenvalues (m^2) are real, and 2) the eigenfunctions form a complete, orthogonal set. Although (2.5) cannot be put into Sturm-Liouville form (because of the singularities inside the domain), it can be shown (Holl, 1970) that its eigenvalues and eigenfunctions have these same properties. This agreement between the character of the differential equations

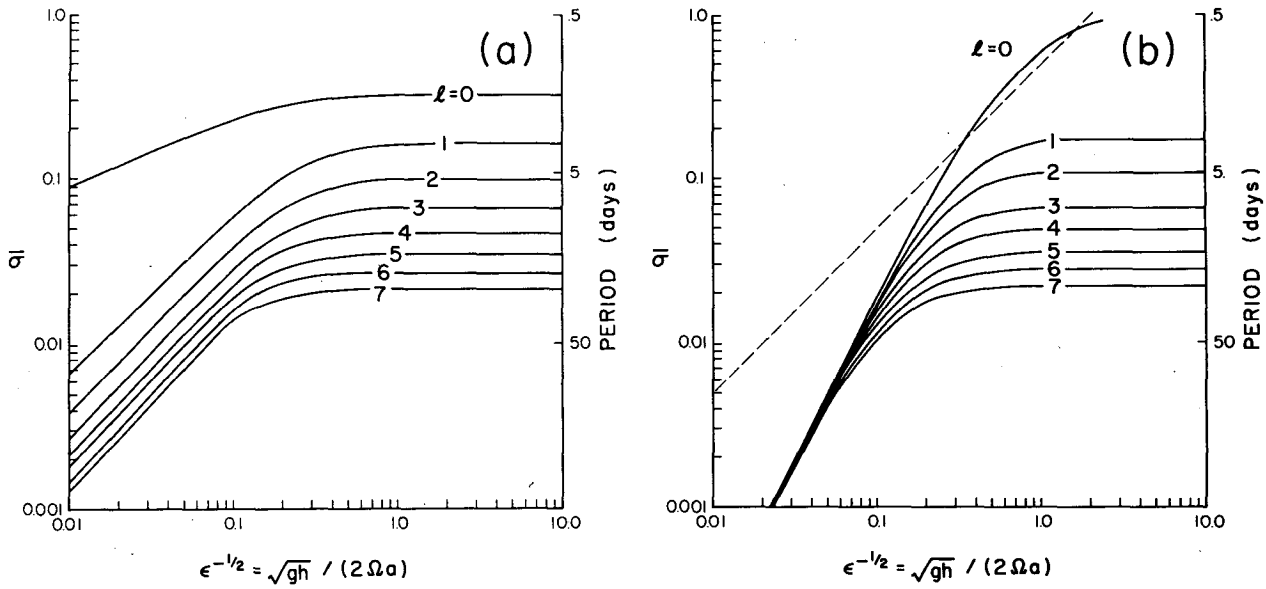

FIG. 3. Eigenfrequencies of Rossby modes with $s = 2, l = 0$–7 and $h > 0$ on the sphere (a) and on the polar plane (b) as a function of meridional index. Below the dashed line in (b), the approximation $\eta^2 r^2 \leq 0.1$ ($\ll 1$) will be good out to $r = a$.

would seem to be essential if we are to successfully replace the spherical geometry.

b. Boundary conditions: $s \geq 1$

Eigenvalues and eigenfunctions of (3.9) were calculated and compared with corresponding solutions on the sphere shown in Longuet-Higgins (1968) and with solutions computed using computer routines developed by A. Kasahara at NCAR. The cases $h \gtrless 0$ are treated separately. Solutions on the sphere are constructed to be either symmetric or antisymmetric about the equator, where $f(\theta)$ changes sign. For the purpose of comparison, we pose boundary conditions on the polar plane solutions which will make the solutions symmetric or antisymmetric about a radius r_c which will serve as an equator. In the analytical study, where f is a constant (2Ω), we take $r_c = 10\,000$ km, corresponding to the pole-to-equator distance on the earth. To assess the impact of setting f = constant, Eq. (3.9) can be put into finite-difference form and solved numerically with f and β fully varying functions of r.

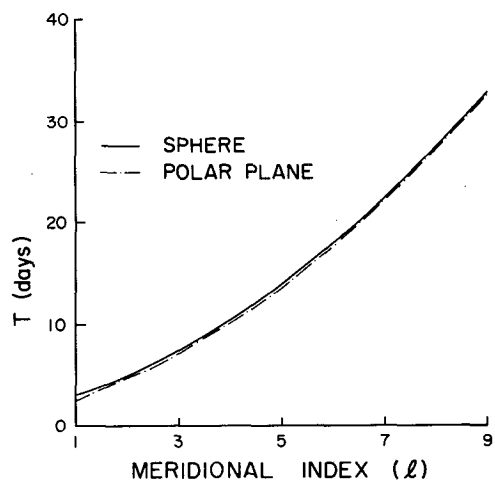

FIG. 4. Period of Rossby modes with $s = 2$ in a nondivergent, barotropic atmosphere as a function of meridional index.

The symmetry of a given mode will be indicated by l = number of zeros of v_r in the interval $-\pi/2 < \theta < \pi/2$ on the sphere (imagine replacing spherical geometry by polar planes at each pole to define l for the polar plane); even l corresponds to symmetric modes. For modes with l odd, we demand that $v_r \approx J_s(mr)/r$ vanishes at $r = r_c$. Hence,

$$J_s(mr_c) = 0,$$

$$\Rightarrow mr_c = j_{sk}, \text{ the } k\text{th zero of } J_s,$$

$$\text{where} \quad k = (l + 1)/2,$$

$$\Rightarrow m^2 = (j_{sk}/r_c)^2.$$

This condition, along with the definition of m^2 given in (3.10), allows us to compute σ given h (free modes) or h given σ (forced modes). For those modes symmetric about r_c, we demand

$$\frac{dv_r}{dr} = 0 \text{ at } r_c,$$

$$\Rightarrow J_{s+1}(mr) = \frac{(s-1)}{mr} J_s(mr) \text{ at } r_c.$$

When $s = 1$, therefore, the local extrema of $J_1(mr)/r$

are at the same radii as the zeros of J_2. (We note that this does not give us a boundary condition on the $s = 1, l = 0$ mode. For reasons given below, no further attempt was made to reproduce this mode.) For $s > 1$, zeros of the function $F = mrJ_{s+1}(mr) - (s - 1)J_s(mr)$, together with specification of r_c give values of m and hence again of σ or h. (For example, if $l = 4$, we set the third local extremum of v_r at $r = r_c$, i.e., seek the third zero of F.)

c. Comparison of eigenvalues when $h > 0$; $s \geq l$

Fig. 3a shows the relationships between nondimensional frequency, $\bar{\sigma}$ and $\epsilon^{-1/2}$ on the sphere for the westward propagating ($\bar{\sigma} > 0$) Rossby modes with $s = 2$. Similar graphs have been constructed for $s = 1$, 3 and 4 but space does not permit presenting them all. Fig. 3b shows the corresponding results on the polar plane. We note the following:

(i) The results are similar in a qualitative sense, inasmuch as $\bar{\sigma}$ is in both cases a monotonic function of h, tending to zero as $h \to 0$ and to a finite limit as $h \to \infty$.

(ii) On the sphere as $h \to \infty$ the eigenfrequencies tend to a constant value. This value, of course, is the frequency of a free oscillation in a barotropic, nondivergent atmosphere, given by

$$\bar{\sigma} = \frac{s}{[n(n+1)]}, \quad \text{where} \quad n - s = l.$$

On the polar plane, the same behavior is noted where now

$$\bar{\sigma} = \frac{s}{m^2 a^2}, \quad \text{with} \quad m^2 = (j_{sk}/r_c)^2.$$

Fig. 4 shows a comparison of limiting periods for the two geometries when $s = 2$ (see also Haurwitz, 1975b, Table 1). The periods on the polar plane are shorter than those on the sphere, although the errors are small.

We note that given s, the error decreases as l increases, while for fixed l, the approximation is best at small s (not shown). To understand this behavior, normalized solutions (v_r, v_λ, Φ) were constructed such that the total energy (E = kinetic + potential) in the domain $0 \leq r \leq r_c$ is 0.5, loosely corresponding to the globally integrated total energy of a mode on the sphere equal to unity (Kasahara, 1976; Longuet-Higgins, 1968). For a given mode, the total energy in 250 km wide radial bands was calculated and its cumulative value was plotted, ranging from zero at the pole to 0.5 at 10 000 km. The shape of the resulting curve is thus an indicator of how much of the disturbance energy is located near the pole. Fig. 5 shows one such plot for $s = 2$ and $l = 0$–7. Clearly, disturbances with large meridional scale have little energy near the pole. Similar plots for

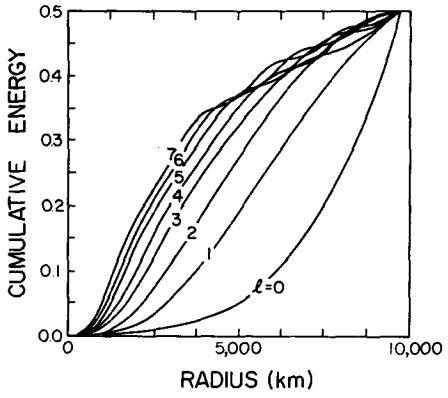

FIG. 5. Cumulative total energy as a function of radius for Rossby modes with $s = 2$, $l = 0$–7 and $\epsilon = 0$.

small l modes, when $s = 1$, 3 and 4, show that most of the disturbance energy is toward the equator, where the approximation involving the geometry and the value of f are worst; it is for this reason that no attempt was made to model the $s = 1$, $l = 0$ mode. Examination of the plots of cumulative energy versus radius for $s = 1$–4 and $l = 0$–7 indicates that as l increases at fixed s, the disturbance energy becomes more concentrated near the pole while the reverse is true as s increases at fixed l.

(iii) As Figs. 3a and 3b show, frequencies are lower on the polar plane than on the sphere at equivalent depths $\leq$ 10 km, and substantial differences manifest themselves at small h. As is well known, solutions with small, positive h tend to be confined to the tropics and we do not expect the polar plane geometry to do well in this region. On the sphere, as $h \to 0$, we may write $\bar{\sigma} \approx s\epsilon^{-1/2}/(2l + 1)$ (Longuet-Higgins, 1968), whereas on the polar plane as $h \to 0$, $\bar{\sigma} \to 0$ approximately as $\bar{\sigma} \approx s\epsilon^{-1}$. Returning to (3.10), we see that in the frequency equation, as $h \to 0$, the term involving m^2 (i.e., the latitudinal structure) drops out; so given s, the relationship between $\bar{\sigma}$ and ϵ is the same for all l at small h.

(iv) For a specific comparison, we consider results when $\epsilon = 10$ ($h = 8.75$ km) shown in Fig. 6. We note that waves on the polar plane move more slowly than those on the sphere. The error at $(s,l) = (1,4)$ is 14%, while for $(s,l) = (3,4)$ it is 2.5%. We note the same variation in errors as s and l vary as was reported for the nondivergent case.

(v) Finally, we note the impact of setting f = constant. As mentioned above, (3.9) is put into finite-difference form and f and β are given by $f = 2\Omega \times \cos\psi$ and $\beta = -(2\Omega/a)\sin\psi$, where $\psi = r/a$. It is found that the $\bar{\sigma}$, $\epsilon^{-1/2}$ curves resemble those on the sphere more closely when f is variable. Not surprisingly, the biggest improvement is noted at small h, representing modes confined near the equator. For example, the $s = 2$, $l = 3$ mode with

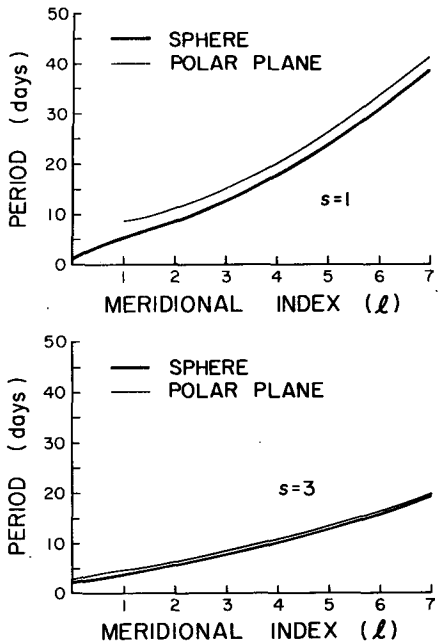

FIG. 6. Periods of Rossby modes in an atmosphere with $h = 8.75$ km ($\epsilon = 10$) as a function of l.

$h = 875$ m, has a period $T = 17.3$ days on the sphere. On the polar plane, the period is reduced from 31.8 to 20.4 days when we allow f to vary.

d. Comparison of eigenvalues when $h < 0$: $s \geq 1$

Figs. 7a and 7b show the variations of $\bar{\sigma}$ with ϵ, for $s = 2$ in both geometries. Odd modes are shown. As with the $h > 0$ cases, there are qualitative similarities, namely, for the westward propagating modes $\bar{\sigma}$ tends to (different) finite limits as $h \to -0$ and $-\infty$, the latter being the same as when $h \to +\infty$. In between, $\bar{\sigma}$ is a monotonic function of h. For the eastward propagating modes, we note that in both geometries, eigenvalues exist only for values of $-\epsilon$ greater than a critical value, $-\epsilon_c$. In the region $-\infty < \epsilon < \epsilon_c$ there are two values of $\bar{\sigma}$, given $-h$. One branch of the solution tends to a finite limit as $h \to -0$, while the other goes to zero as $\bar{\sigma} \approx s\epsilon^{-1}$, in agreement with the spherical case. Quantitative differences are now outlined, first for the westward propagating modes ($\bar{\sigma} > 0$).

(i) Longuet-Higgins (1968) points out that for the sphere as $h \to -0$, $\bar{\sigma} \to 1$, $\bar{\sigma}$ always being less than 1. On the polar plane, values of $\bar{\sigma}$ in excess of 1 are noted, $\bar{\sigma}$ tending to 2.4 and 1.6 for $s = 1$ and 2, respectively. As mentioned in Section 3, we can only assume that results for which $|\epsilon\bar{\sigma}^2/s^2|(r/a)^2 \ll 1$ is valid will be a good approximation to the true results. Below the dotted lines superimposed on the $\bar{\sigma}$, ϵ curves, this approximation is good for $r \leq a$. The behavior of the westward propagating solutions at lower values of $|h|$ (larger $|\epsilon|$) is not, therefore, expected to bear close relation to that on the sphere. This may explain both the limiting frequencies (as $h \to -0$) being too high and also the excessively sharp dips in the curves as $-h$ increases.

It may be desirable to have a better representation of these westward propagating modes with small, negative h, especially as these modes tend to be confined to the polar regions. To do this, we can revert to (3.8) and make the assumption $\eta^2 r^2 \gg 1$, i.e., $\bar{\sigma}\epsilon^2 \gg (sa/r)^2$, which will be satisfied at large $\bar{\sigma}$ and $|\epsilon|$ (small $|h|$). Assuming $h < 0$, Eq. (3.8) may be written

$$\frac{d^2R}{dr^2} + \frac{dR}{rdr} + \left(n^2 - \frac{\alpha^2}{r^2}\right)R = 0, \qquad (4.1)$$

where

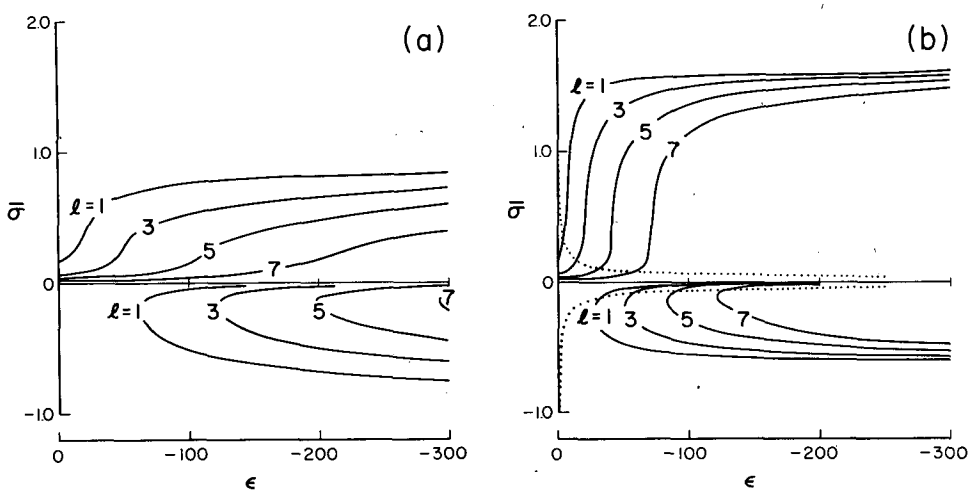

FIG. 7. Eigenfrequencies of lowest anti-symmetric modes ($l = 1, 3, 5, 7$) with $s = 2$ and $h < 0$ on the sphere (a) and on the polar plane (b) as a function of ϵ. Along the dotted lines in (b), $\eta^2 r^2 = 0.1$ at $r = a$. The approximation $\eta^2 r^2 \leq 0.1$ ($\ll 1$) is good between the dotted lines.

$$n^2 = s/\bar{\sigma} - \epsilon(1 - \bar{\sigma}^2), \qquad (4.2)$$

r is dimensionless (scaled by a), and

$$\alpha^2 = s^2 - 2s/\bar{\sigma} + 1. \qquad (4.3)$$

The solution is thus $R = J_\alpha(nr)$. Examination of (4.2), when n is specified by the symmetry boundary condition at the equator, shows that as $h \to -0$, $\bar{\sigma} \to \pm 1$, as on the sphere. Furthermore, comparison of the expressions for ϵ in terms of $\bar{\sigma}$ and m^2 (when $\eta^2 r^2 \ll 1$) and of $\bar{\sigma}$ and n^2 (when $\eta^2 r^2 \gg 1$) reveals that the latter approximation will yield results closer to their spherical counterparts.

(ii) We further note that the solutions remain distinct on the polar plane as $h \to -0$, whereas on the sphere, symmetric and antisymmetric modes become paired (not shown). On the sphere as $\epsilon \to -\infty$, modes become increasingly confined to polar latitudes, with exponentially decreasing amplitudes as the equator is approached. A pair of symmetric and antisymmetric solutions are then either in phase or π out of phase with each other near the poles and share the same eigenfrequency. On the polar plane, the solutions at small $-h$ do not become exponentially small near the equator, so this pairing of eigenfrequencies is not expected.

(iii) For the eastward propagating modes ($\bar{\sigma} < 0$), we again note that solutions are not paired at small $-h$ for the same reasons as outlined in (ii) above. Also, for the higher frequency branch, the limiting values of $\bar{\sigma}$ as $h \to -0$ are lower than those on the sphere, but as discussed above, the geometrical approximations are not good here. We expect the lower frequency eastward propagating modes to be well approximated on the polar plane since they satisfy the criterion $|\eta^2 r^2| \ll 1$, although as Fig. 7 shows, equivalent depths on the polar plane are higher than on the sphere.

(iv) As noted by Jones (1972), the eigenfrequencies on the sphere may become complex at large, negative values of h. This behavior is also found on the polar plane. Referring to Fig. 7b, at small, negative h, there are two distinct, eastward propagating modes. As $|h|$ increases, the solutions converge and eventually join to form a complex conjugate pair. The value of $-\epsilon$ beyond which Longuet-Higgins (1968) found no solutions may thus be interpreted as the value of $-\epsilon$ at which complex values first appear. The behavior of the complex solutions is qualitatively the same as on the sphere [see Figs. 2–4 in Jones (1972)]. As $h \to -\infty$, Re(σ) tends to a constant value while $|\text{Im}(\sigma)| \to \infty$.

e. Comparison of eigenfunctions: $s \geq 1$

In Figs. 8 and 9 we show the radial dependencies (R,Λ,ϕ) of (v_r,v_λ,Φ) on the polar plane along with those of (u,v,ϕ) on the sphere for the cases $(s,l,\epsilon) = (1,4,10)$ and $(2,3,10)$. The periods of these disturbances are 17.6 and 8.6 days, respectively, on the sphere and 19.6 and 9.8 days, respectively, on the polar plane. As mentioned in Section 4c, solutions on the polar plane were normalized in approximately the same fashion as were those on the sphere.

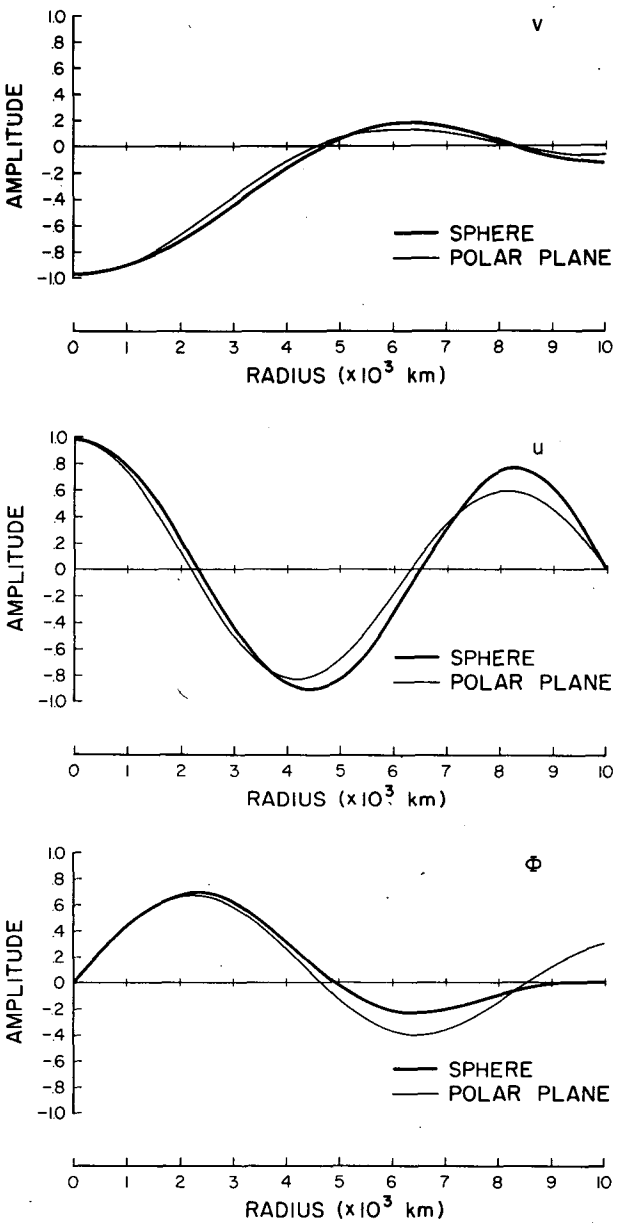

FIG. 8. Amplitude of meridional wind (a), zonal wind (b) and geopotential (c) as a function of radius for the case $(s,l,\epsilon) = (1,4,10)$.

(i) Considering first the (1,4,10) mode, we find a close correspondence between results in the two geometries, even toward lower latitudes. The nodes in (v_r,v_λ,Φ) are all observed to be close to their "true" locations, as are the extrema.

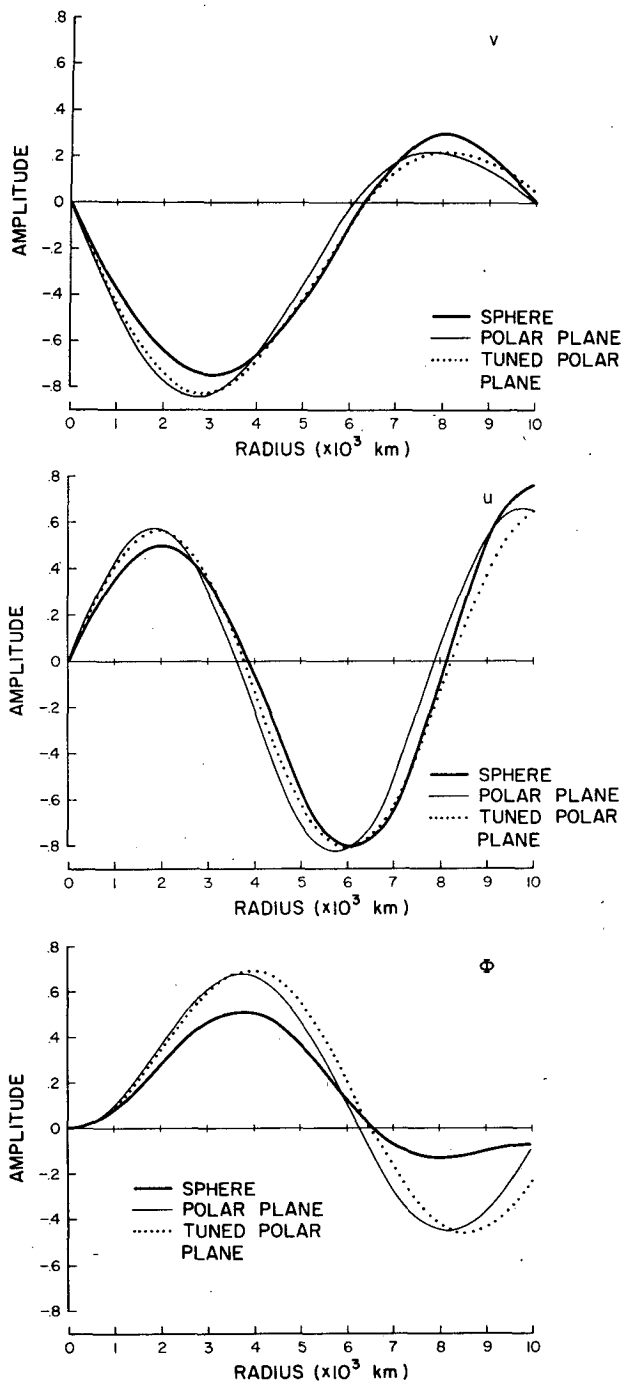

FIG. 9. As Fig. 8, except with $(s,l,\epsilon) = (2,3,10)$.

The geostrophic relations for the polar plane may be written as

$$fv_r = -\frac{\partial \Phi}{r\partial\lambda} \quad \text{and} \quad fv_\lambda = \frac{\partial \Phi}{\partial r}, \quad \text{i.e.,}$$

$$R = -\frac{is\phi}{fr} \quad \text{and} \quad \Lambda = \frac{1}{f}\frac{d\phi}{fr}. \qquad (4.4)$$

It can be seen that these relationships are well satisfied in both geometries for these long-period disturbances. We note from (4.4) that allowing f to vary as sin(latitude) would give a lower value of f and thus of ϕ and $d\phi/dr$ near the equator, where at present, the amplitude of ϕ is not well modeled on the polar plane.

(ii) The (2,3,10) mode is similarly well modeled on the polar plane again with the exception of the geopotential in low latitudes.

Following the discussion in Section 4b(ii), we expect on energetic grounds that for a fixed l as s increases, the errors become larger. This was confirmed by looking at modes with $s = 1$–4 and $l = 1$–7 (not shown) and is somewhat borne out by comparison of Figs. 8 and 9 (although they have different values of l).

(iii) In previous studies (LeBlond, 1964; Haurwitz, 1975a,b), a boundary condition of symmetry or antisymmetry at the equator was replaced by one of setting the node in v_r closest to the pole at a specified radius. In so doing, of course, we can generally no longer use the index l to define meridional wavenumber, nor can we term disturbances symmetric or antisymmetric. In Fig. 9, we also show the eigenfunctions derived by setting the aforementioned node in v_r at the radius, where the node on the sphere occurs. There is a marginal improvement in the solution at middle and high latitudes. We observe also that the predicted frequencies in this "tuned" model are closer to their spherical counterparts.

(iv) Referring to (3.11), we see that given s and l, the solution for v_r remains fixed (in shape, but not amplitude) as h changes, since $m = (j_{sk}/r_c)^2$ is fixed by the boundary condition. Varying h merely varies σ, with m unchanged, as (3.10) shows. Hence, as $h \to +0$, the solution for v_r does not become confined near the equator, as Longuet-Higgins (1968) showed will happen on the sphere. Similarly, as $h \to -0$, v_r will not become confined to the polar regions. The solutions for v_λ and Φ may, however, change shape as h and σ vary, although the changes are by no means as drastic as those on the sphere. It is found that on the polar plane as $h \to +0$, the total energy of a given mode is indeed located further from the pole. However, since the geometrical approximation is worst at the equator, and since we have taken f = constant, we conclude that only those modes with $\epsilon \lesssim 10$ are well represented on the polar plane. Similarly, treating the cases with $h < 0$ as a forced problem, as $\bar{\sigma} \to \pm 1$ for the two high-frequency branches of the solution, the disturbance energy does become confined to higher latitudes, but in the limit, disturbances do not become vanishingly small near the equator. For the slower moving, eastward propagating modes, the eigenfunctions and their behavior as $h \to -0$ (and

$|\bar{\sigma}| \to 0$) are better modeled. Solutions obtained are qualitatively similar to those shown in Longuet-Higgins (1968, Figs. 24 and 27) except for the behavior near the equator. For $h < 0$, therefore, modes with $|\bar{\sigma}| \lesssim 0.1$ are best represented on the polar plane. We note briefly that allowing f to vary in the finite-difference version of (3.9) produces the desired confinement in v_r (depending upon the sign of h), as does the approximation $|\eta^2 r^2| \gg 1$, valid for the two higher frequency solutions at negative h.

f. The s = 0 case

For completeness, we consider the case of oscillatory, stationary solutions ($s = 0$). Taking $\lim_{s\to 0}$ (3.8) gives

$$\frac{d^2R}{dr^2} + \frac{1}{r}\frac{dR}{dr} + \left(\frac{\sigma^2 - f^2}{gh} - \frac{1}{r^2}\right)R = 0, \quad (4.5)$$

with the solution

$$R = J_1(mr) = v_r, \quad \text{where} \quad m^2 = (\sigma^2 - f^2)/gh. \quad (4.6)$$

The frequency equation is now

$$m^2 = \frac{\sigma^2 - f^2}{gh} = \left(\frac{j_{1k}}{r_c}\right)^2,$$

giving

$$\sigma = \pm(m^2 gh + f^2)^{1/2}. \quad (4.7)$$

There is a third solution with $s = \sigma = 0$ which yields

$$R^* = 0 \quad \Rightarrow \text{zonal motion}$$

$$f\Lambda = \frac{d\phi}{dr} \quad \Rightarrow \text{geostrophic motion.}$$

The other solutions are a pair of high-frequency gravity modes. For $h < 0$, as $h \to -0$, $\bar{\sigma} \to 1$ and at $-h = f^2/m^2 g$, $\bar{\sigma} = 0$. For $-h$ larger, $\bar{\sigma}$ is imaginary. These results concur qualitatively with those on the sphere (Longuet-Higgins, 1968, Fig. 16). For $h > 0$, $\bar{\sigma} \to \infty$ as $h \to \infty$ while $\bar{\sigma} \to 1$ as $h \to +0$. On the sphere as $h \to +0$, $\bar{\sigma} \to 0$. This discrepancy is resolved by noting that on the sphere as $h \to 0$, the eigenfunctions become confined near the equator where f is small; so on the sphere, $h \to 0$ and $f \to 0$ and so $\bar{\sigma} \to 0$, whereas on the polar plane, f remains equal to 2Ω. The eigenfunctions for $s = 0$ were not computed.

5. Conclusions

It has been shown that for certain disturbances, the polar-plane geometry does well in emulating results on a spherical earth. If we make the assumptions outlined in Section 3, namely, $\eta^2 r^2 \ll 1$ and f = constant (2Ω), we obtain a (relatively) simple cubic frequency equation for free motions. The eigenfunctions can then be discussed in terms of a single Bessel function. Writing the governing equation in finite-difference form allows us to assess the impact of setting f = constant, although in letting f and β vary, we lose the analytic simplicity of the model.

For positive equivalent depths, the approximation is best when $\epsilon \lesssim 10$, i.e., when $h \gtrsim 8.75$ km. The geometry does not do well at small, positive h, for which disturbances on the sphere become confined to equatorial regions. This shortcoming seems to be due as much, if not more so, to the erroneous value of f in equatorial regions as it is to the geometry. The same is true of the eigenfunctions. The winds are well modeled at all latitudes, although at large radii this is somewhat fortuitous, since the amplitude of ϕ is poorly modeled. In the simple, analytical model, the confinement of solutions near the equator (as $h \to +0$) or near the pole (as $h \to -0$) does not occur, since the solution for v_r is independent of variations in h or σ for a given s and l. However, within the bounds outlined above, the representation is generally good and suggests that this approximation may be useful in studying the behavior of the atmosphere at high latitudes.

Acknowledgments. The authors wish to thank Bernhard Haurwitz for his suggestions and for reviewing the manuscript. We also acknowledge the National Center for Atmospheric Research for computing facilities used in this research, Polly Cletcher for typing the manuscript and Mark Howes for drafting the figures. The work was funded by the National Science Foundation under Grants ATM 77-07096 and ATM 78-12212.

APPENDIX

List of Symbols

a	earth's radius
c_p	specific heat at constant pressure
f	Coriolis parameter
g	gravitational acceleration
h	equivalent depth
l	index of latitudinal wavenumber
r	distance on the sphere from the pole
R^*	gas constant for dry air
s	longitudinal wavenumber
t	time
T	temperature ($\bar{T}$ mean, T' perturbation)
u'	perturbation eastward velocity [$=v_\lambda'$]
$u' = U(\theta)Y(z)$,	$v_\lambda' = \Lambda(r)Z(z)$
v'	perturbation northward velocity [$=-v_r'$]
$v' = V(\theta)Y(z)$,	$v_r' = R(r)Z(z)$
w'	perturbation upward velocity [$=dz/dt$]
z	$-\ln(p/p_0)$
β	df/dr
Γ	static stability parameter
ϵ	Lamb's parameter [$=4\Omega^2 a^2/gh$]
η^2	$\sigma^2/s^2 gh$

θ latitude
κ R^*/c_p
λ longitude
σ frequency
Φ' perturbation geopotential
$\Phi' = \Psi(\theta)Y(z), \quad \Phi' = \phi(r)Z(z)$
ψ colatitude
Ψ_n^s Hough function
Ω earth's rotation rate.

REFERENCES

Abramowitz, M., and I. Stegun, 1972: *Handbook of Mathematical Functions*. Dover, 1045 pp.

Chapman, S., and R. S. Lindzen, 1970: *Atmospheric Tides*. D. Reidel, 200 pp.

Dickinson, R. E., 1968a: Planetary Rossby waves propagating vertically through weak westerly wind wave guides. *J. Atmos. Sci.*, **25,** 984–1002.

——, 1968b: On the exact and approximate linear theory of vertically propagating planetary Rossby waves forced at a spherical lower boundary. *Mon. Wea. Rev.*, **96,** 405–415.

Flattery, T. W., 1967: Hough functions. Tech. Rep. No. 21, Dept. Geophys. Sci., The University of Chicago, 175 pp.

Haurwitz, B., 1975a: Long circumpolar atmospheric waves. *Arch. Meteor. Geophys. Bioklim.*, **A24,** 1–18.

——, 1975b: Long waves in the polar atmosphere. *Climate Arctic*, Vol. 1, 175–180.

Holl, Peter, 1970: Die vollständigkeit des orthogonalsystems der Houghfunktionen. *Nach. Akad. Wissens. Göttingen II. Math.-Phys. Kl.*, **7,** 159–168. [English translation (The completeness of the orthogonal system of the Hough functions) by B. Haurwitz. Available from Dept. of Atmos. Sci., Colorado State University.]

Holton, J. R., 1975: *The Dynamic Meteorology of the Stratosphere and Mesosphere. Meteor. Monogr.*, No. 37, 218 pp.

Jones, W. L., 1972: Unstable solutions to Laplace's tidal equation with negative equivalent depth. *J. Atmos. Sci.*, **29,** 457–462.

Kasahara, A., 1976: Normal modes of ultralong waves in the atmosphere. *Mon. Wea. Rev.*, **104,** 669–690.

LeBlond, P. H., 1964: Planetary waves in a symmetrical polar basin. *Tellus*, **16,** 503–512.

Lindzen, R. S., 1967: Planetary waves on beta-planes. *Mon. Wea. Rev.*, **95,** 441–451.

Longuet-Higgins, M. S., 1968: The eigenfunctions of Laplace's tidal equation over a sphere. *Phil. Trans. Roy. Soc. London*, **262A,** 511–607.

Matsuno, T., 1970: Vertical propagation of stationary planetary waves in the winter Northern Hemisphere. *J. Atmos. Sci.*, **27,** 871–883.

——, 1971: A dynamical model of the stratospheric sudden warming. *J. Atmos. Sci.*, **28,** 1479–1494.

Simmons, A. J., 1974: Planetary-scale disturbances in the polar winter stratosphere. *Quart. J. Roy. Meteor. Soc.*, **100,** 76–108.

Thomas, J. H., and R. A. Lux, 1978: Refraction of Rossby waves on a multiple β-plane. *Dyn. Atmos. Oceans*, **2,** 411–426.